Porous activated carbons derived from bamboo pulp black liquor for effective adsorption removal of tetracycline hydrochloride and malachite green from water

Mengyuan Yang
Sichuan University
Ce Cui
Sichuan University
Li Liu
Sichuan University
Lanling Dai
Sichuan University
Wenhao Bai
Sichuan University
Jianyu Zhai
Sichuan University
Shan Jiang
Sichuan University
Weijie Wang
Sichuan University
Erhui Ren
Sichuan University
Cheng Cheng
University of Leeds
Ronghui Guo (ronghuiguo214@126.com)
Sichuan University

Research Article

Keywords: Bamboo pulp black liquor, porous carbon, tetracycline hydrochloride, malachite green, adsorption

Posted Date: March 17th, 2022

DOI: https://doi.org/10.21203/rs.3.rs-1423230/v1

Porous activated carbons derived from bamboo pulp black liquor for effective adsorption removal of tetracycline hydrochloride and malachite green from water

Mengyuan Yang[1,2], Ce Cui[1,2], Li Liu[3], Lanling Dai[1,2], Wenhao Bai[1,2], Jianyu Zhai[1,2], Shan Jiang[1,2], Weijie Wang[1,2], Erhui Ren[1], Cheng Cheng[4], Ronghui Guo[1,2*]

1. College of Biomass Science and Engineering, Sichuan University, Chengdu 610065, China
2. Yibin Industrial Technology Research Institute of Sichuan University, Yibin, Sichuan, China
3. College of Chemistry, Sichuan University, Chengdu 610065, China
4. School of Chemical and Process Engineering, University of Leeds, Leeds, United Kingdom

Abstract: As a kind of waste water produced by papermaking industry, bamboo pulp black liquor (BPBL) discharged into water cause serious environmental problems. In this work, BPBL was successfully converted into porous carbon after activation with KOH through one-step carbonization, and adsorption properties of porous carbon derived from bamboo pulp black liquor (BLPC) for tetracycline hydrochloride (TCH) and malachite green (MG) were studied. Adsorption capacity of BLPC for TCH and MG arrive at 1047 mg/g and 1277 mg/g due to its large specific surface area of 1859.08 m^2/g, respectively. Kinetics and isotherm data are well fitted to the pseudo-second-order rate model and Langmuir model, respectively. Adsorption experiments and characterizations reveal that the adsorption mechanism involves in TCH and MG adsorption on BLPC mainly depends on the synergistic effect of pore filling, H-bonding, π-π interactions and weak electrostatic interactions. In addition, BLPC shows excellent photo-thermal property and improves its adsorption properties for TCH and MG under near-infrared irradiation. The synthesized BLPC with high adsorption efficiency, good recovery ability, improved adsorption under near-infrared irradiation can be promising and effective adsorbents for TCH or MG or other pollutes.

Keywords: Bamboo pulp black liquor, porous carbon, tetracycline hydrochloride, malachite green, adsorption

1. Introduction

In recent years, water contamination has become an imperative global environment problem with the fast development of urbanization, industry and healthcare. Especially, various waste water containing antibiotic and dyes have been emitted from pharmaceutical factory and textile dyeing [1]. Tetracycline hydrochloride (TCH), as a kind of antibiotics, has been used for the treatment and prevention of diseases for human and animals[2]. However, most of TCH ingested by animals is excreted from the body through urine, and then enters rivers and oceans through ecological circulation, which in turn leads to creation of drug-resistant bacteria and pollution for the environment, therefore affects ecosystems

*Corresponding Author. Ronghui Guo, E-mail address:ronghuiguo214@126.com (R. H. Guo)

and human health[3]. Additionally, malachite green (MG), a blueish green cationic dye has been widely used to impart color in textile and leather industries. MG shows a distinct color even at very low concentrations and greatly affects photosynthesis in aquatic plants. Currently, various methods, such as photocatalytic degradation [4, 5], electrochemical degradation[6, 7], biodegradation[8], advanced oxidation processes[9], adsorption[10, 11] and membrane separation[12], have been developed to removal of TCH and MG in wastewater. Among these technologies, adsorption method has attracted widespread interest due to lack of secondary pollution, high efficiency and low cost, and easy operation[13]. Nowadays, a variety of adsorbents have been used for removal of TCH and MG such as graphene oxide[14], biochar[15], MOFs[16], porous carbon[17] and their derivatives. Among these materials, porous carbon has been widely used as adsorbent for TCH and MG removal due to its large specific surface area, excellent porous structure, low cost, abundant surface functional groups and abundant raw materials.

Bamboo pulp black liquor (BPBL) is waste from the conventional kraft pulping process in the paper industry. These black liquors exist in industrial wastewater and can be easily released into the hydrosphere, therefore affecting water resource. Traditionally, BPBL is burnt to recover the pulping chemicals and energy. In addition, it is rich in lignin, cellulose and hemicellulose, which can be converted into useful products using the organic matter in BPBL. In general, lignin is extracted from BPBL and used to prepare bio-asphalt [18] , super capacitors [19] and activated carbon [20], but these studies only use lignin in BPBL and cannot fully utilize other organic matter. Until now, the conversion of all the organic compounds of BPBL such as lignin, cellulose and hemicellulose to porous carbons and their application still has been little studied, and particularly, there was no relevant report about the research of BPBL derived BLPC for applications in antibiotic and dye wastewater treatment.

In this study, BPBL and KOH were used as raw materials as activators, and various organic compounds in black liquor were fully utilized to prepare high-performance black liquid derived porous carbon (BLPC) from bamboo pulp by one-step method. The structure, morphology and surface functional groups of BLPC were characterized. The effects of mixing ratios of KOH and BPBL and activation temperatures on adsorption properties of BLPC for TCH and MG at were investigated. The dynamics, isotherms and reusability of the BLPC were studied. The effect of near-infrared irradiation on the adsorption of TCH and MG by BLPC was also explored.

2. Experimental

2.1 Materials

Bamboo pulp black liquor (BPBL) was obtained from Huanlong New Materials Co, tetracycline hydrochloride (TCH), malachite green (MG), hydrochloric acid (HCI) and potassium hydroxide (KOH, AR) were purchased from Chengdu Chron Chemicals Co. LTD.

2.2. Preparation of BLPC

BPBL were used as raw material for porous carbon and KOH was utilized as activating agent. First, KOH and 20 g BPBL of different mass (0-3.6 g) were added to 10 mL deionized water to make KOH and BPBL mix evenly. After that, the mixture was dried in oven and was then activated in a tube furnace by a sequentially increasing temperature to the

target temperature (750−850 °C) at a heating rate of 5 °C min^{-1} under N_2 atmosphere for 1 h to obtain the bamboo pulp black liquid porous carbon (BLPC). The obtained BLPC products were fully grinded and thoroughly washed with 1 mol /L HCl solution to remove any inorganic salts and further washed with deionized water until pH was neutral. Finally, the product was dried at 105 ° C for 12 h. The samples are named BLPC-T-X, where T (750, 800 and 850 ℃) stands for activation temperature and X (0, 12, 15 and 18 %) means the ratio of KOH to BPBL.

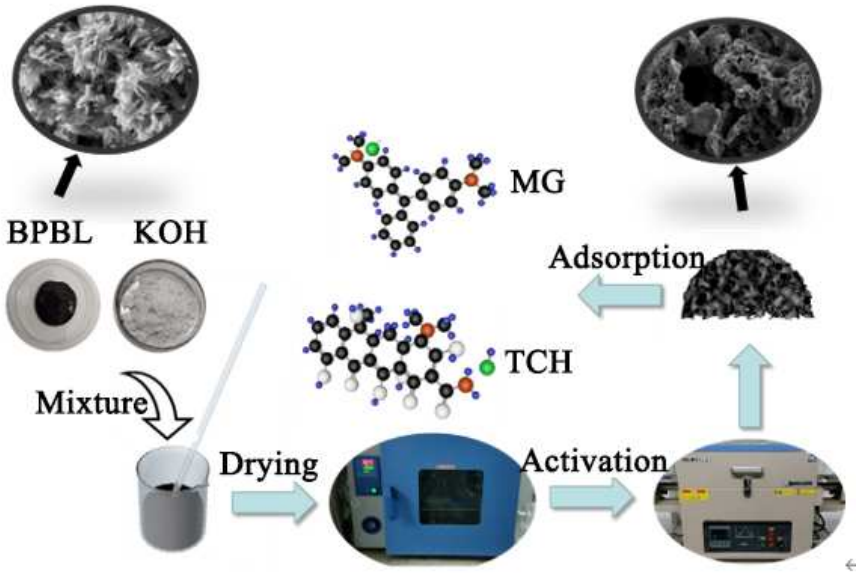

Fig. 1 Preparation process of BLPC

2.3 Characterization

Surface morphologies of the BPBL and BLPC were observed at an acceleration voltage of 10 kV and 10 mm of working distance by SEM (JSM-5900LV). Chemical functional groups of the samples were identified by fourier transform infrared spectroscopy (IRTracer-100). BLPC were tested by XRD (X'Pert Pro MPO) at a scan rate of 5° per minute in an angle range of 5-80°. N_2 adsorption-desorption isotherms of the prepared adsorbents were measured at 77 K (Gemini VII 2390).

2.4. Adsorption experiments

TCH and MG adsorption experiments were conducted to evaluate adsorption performance of BLPC. Effects of different pH, temperature and pollutant concentration on TCH and MG adsorption of BLPC were studied. In order to investigate adsorption kinetics, a batch of experiments were conducted by adding 30 mg of BLPC-T-X into the TCH and MG solutions (30 mL) with different initial concentrations of 1000 and 1500 mg/L at 288, 298 and 308 K for different designated interval time, respectively. Different initial concentrations (5,10,20,30,40,60,80,100 and 120 mg/L) at three different temperatures (288,298 and 308 K) for 24 h were adopted to study adsorption equilibrium property. The final concentrations of TCH and MG were determined by UV spectrophotometer (UV-2450, Shimadzu, Japan) at 357.0 nm and 617.0 nm respectively. Adsorption amounts of TCH and MG were calculated according to Equations (1) and (2).

$$Q_e = \frac{V(C_0 - C_e)}{M} \quad (1)$$

$$Q_t = \frac{V(C_0 - C_t)}{M} \quad (2)$$

Where C_o and C_e (mg/L) are the initial and ultimate concentrations, respectively. C_t (mg/L) is the remaining contaminant concentration at time t (min). V (mL) is the solution volume and M (mg) is the weight of adsorbent.

30 mg BLPC was added to 30ml TCH and MG solutions (C_0 = 1500mg/ L), respectively. The pH values of TCH solution and MG solution were adjusted to 5-9 and 3-11 with 0.05 mol /L HCl and 0.05 mol /L NaOH, respectively. The effects of BLPC on the adsorption of TCH and MG at different pH values were investigated after adsorption at 298 K for 24 h.

100 mg BLPC was added to 100 mL TCH and MG solution (C_0 = 1500mg/ L) and reacted for 24h. The BLPC was filtered, washed, and placed in 100 mL ethanol under ultrasonic irradiation for 30 min for desorption. The regenerative BLPC was dried for 24 h and then added to TCH and MG solutions to evaluate regeneration efficiency.

BLPC adsorption experiment and photo-thermal temperature of BLPC were performed under 250W near-infrared light at room temperature (25℃), and the surface temperature of BLPC was recorded by infrared imager. Distance between BLPC surface and infrared light (40 cm, 50 cm and 60 cm) was adjusted to measure photothermal performance and effect of near-infrared lamp irradiation on the adsorption properties of porous carbon was evaluated.

3. Results and discussion

3.1 SEM Analysis

Fig. 1 show the surface morphology of BPBL, BLPC-800-0, BLPC-800-12, BLPC-800-15 and BLPC-800-18, respectively. The SEM images revealed noteworthy changes in surface morphology of BPBL after activation. The surface of BPBL shows irregular structure, which is loaded with crystalline salt on organic matter such as lignin (Fig. 2a). However, it is evident from Fig. 1b that carbonization at 800 °C causes elimination of volatile matter from biomass resulting a rough and partially porous surface of BLPC-800-0. Subsequently, a highly porous surface is observed on the BLPC in the presence of KOH after carbonization at 800 °C produced as shown in Fig.1(c-e). The amount of KOH for activation also influences the surface morphology and structure of porous carbon. Abundant pores are observed on the surface of the BLPC-800-12 as shown in Fig. 2c. indicating that appropriate KOH can promote pores. The pore size is further developed when the ratio of KOH increases from 12 % to 15 %. However, excessive KOH leads to the corrosion of carbon structure when the ratio of KOH further increase. The pores of BLPC-800-18 collapse and the pore size increases when the KOH addition ratio is 18 % as shown in Fig. 2e. The activation mechanism of KOH is shown in Equations (3), (4), (5), (6) and (7)[21].

$$6KOH + 2C \rightarrow 2K_2CO_3 + 2K + 3H_2 \quad (3)$$

$$K_2CO_3 \rightarrow CO_2 + K_2O \quad (4)$$

$$4KOH + C \rightarrow 4K + CO_2 + 2H_2O \quad (5)$$

$$K_2O + C \rightarrow 2K + CO \quad (6)$$

$$K_2CO_3 + 2C \rightarrow 2K + 3CO \quad (7)$$

According to the formula, KOH consumes the carbon-containing material in the raw material and pores are formed in the original position at high temperature. Gases are produced during activation, which directly connect the pores with the pores. However, excessive KOH leads to excessive expansion of pores and collapse and the adsorption capacity decreases.

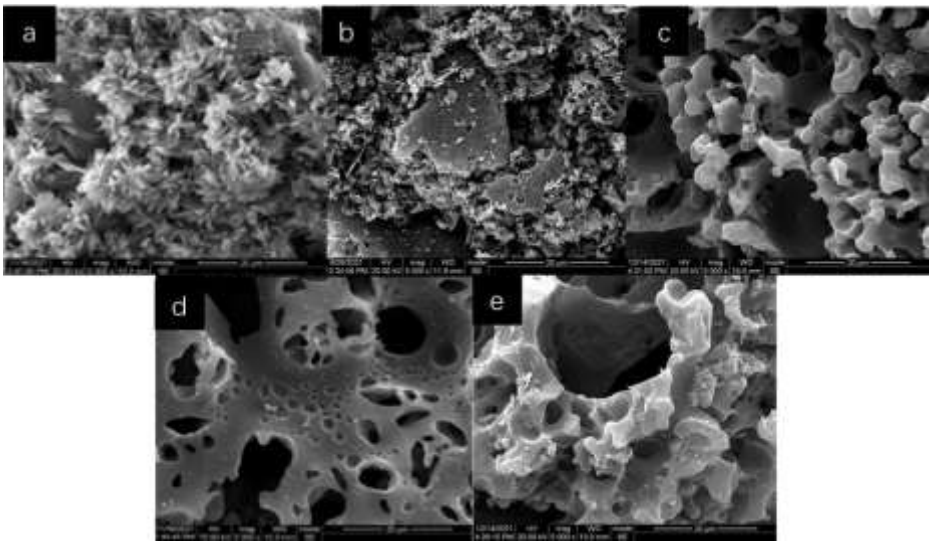

Fig. 2. SEM images of (a) BPBL, (b) BLPC-800-0, (c) BLPC-800-12, (d) BLPC-800-15 and (e) BLPC-800-18.

The N_2 adsorption–desorption isotherms and pore size distribution are shown in Fig. 3 and corresponding specific surface aera and pore volume are presented in Table 1. According to IUPAC classification, isotherms of BLPC can be classified as type I, indicating a large number of micropores and mesopores exist in BLPC, corresponding to langmuir single-layer reversible adsorption process [22]. The specific surface area of porous carbon prepared without KOH activation and BPBL and BPBL activated with 15% KOH are 928.6 cm^2/g and 1859.08 m^2/g, respectively. The result indicates that specific surface areas of porous carbon derived from BPBL with KOH activation is higher than that without KOH activation. The pore volumes of porous carbon prepared without KOH activation and BPBL with 15% KOH activation ranges from 1.96 cm^3/g to 2.11 cm^3/g, respectively. The pore volume arrives at 2.22 cm^3/g when the ratio of KOH is 18 %, indicating that the number of intermediary pores and macropores in porous carbon increases because KOH has pore expanding effect. The specific surface area of BLPC-800-18 is 1494.28 m^2/g, indicating that excessive pore-promoting effect of KOH leads to collapse of micropore and formation of mesopores and macropores, resulting in reduced specific surface area. Fig. 3b shows pore size distribution of the BLPC and the pore sizes of three kinds of porous carbon are mainly below 3 nm, mainly consisting of micropores and mesopores which is conducive to the adsorption of TCH and MG by BLPC.

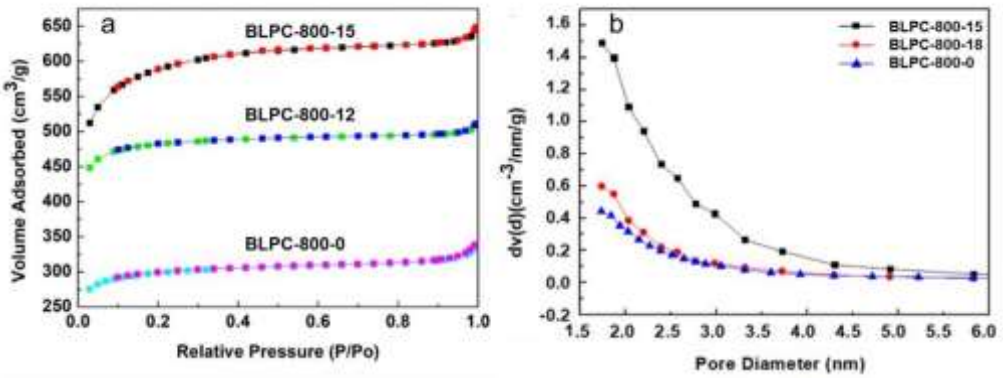

Fig. 3. N_2 adsorption–desorption isotherms (a) and pore size distributions and pore volume of BLPC-T-x (b).

Table 1 The porosity characteristics of BLPC synthesized at different parameters.

Parameters	BLPC-800-15	BLPC-800-18	BLPC-800-0
Specific surface area (m^2/g)	1,859.08 m²/g	1,494.28 m²/g	928.60 m²/g
Total pore volume (cm^3/g)	2.11 cm^3/g	2.22 cm^3/g	1.96 cm^3/g

3. 2 FTIR, Raman and XRD Analyses

FTIR spectra of BPBL, porous carbon derived from BPBL without and with KOH activation are illustrated in Fig. 4a. For BPBL, an obvious peak near 3410 cm^{-1} is attributed to stretching vibration of hydroxyl and carboxyl of BPBL. The strong absorption peak around 2300 cm^{-1} is assigned to characteristics peak of carbon dioxide trapped on the surface of BPBL[23, 24]. The peaks located around 1500 and 1600 cm^{-1} are attributed to symmetric C=C stretching vibrations groups and stretching of carbonyl (C=O) groups of esters and aldehydes. Sharp peak around 1100 cm^{-1} is assigned to C-O-C linkages[25]. The weak absorption peaks at 1597 and 1100 cm^{-1} imply existence of C=O and C-O-C, respectively. The results show that intensities of O-H, C=O and C=C peaks decrease after carbonization. These functional groups can produce hydrogen bond interactions and π-π interactions with TCH and MG and promote the adsorption of TCH and MG.

Raman spectra of porous carbon derived from BPBL without and with KOH activation are shown in Fig. 4b and two distinct peaks can be obviously observed at 1597 (G-band) and 1349 (D-band, disorder) cm^{-1}, corresponding to graphitic and defected carbon, respectively, indicating that main component of as-prepared BLPC is carbon. Generally, the G band means that all sp^2 atoms in the rings and chains show C-C bond stretching[26]. D band is related to the disorder and defects in the crystal structure, which is dominated by defects, distortions and displacements. The intensity ratio between D band and G band (R = D/G) represents the disorder of carbon structure. The D/G specific value of BLPC-800-15 and

BLPC-800-0 are 1.09 and 1.07, respectively, demonstrating that graphitization degree of porous carbon derived from BPBL with KOH activation is lower than that without KOH activation. The porous carbon with lower graphitization degrees contains more oxygen-containing functional groups, higher defect degree, higher specific surface area and a larger number of thin layers than porous carbon with higher graphitization degree, which can effectively improve adsorption capacity of porous carbon[27]. Namely, porous carbon derived from BPBL with KOH activation is better than that without KOH activation.

XRD characteristics were conducted to analyze crystallinity of porous carbon derived from BPBL without and with KOH activation as shown in Fig. 4c. There are two broad peaks in XRD patterns of both porous carbon derived from BPBL without and with KOH activation. The peaks located at 23.5° and 43.0° correspond to (002) and (101) planes of graphite [28], respectively, which was consistent with amorphous and disordered carbon material.

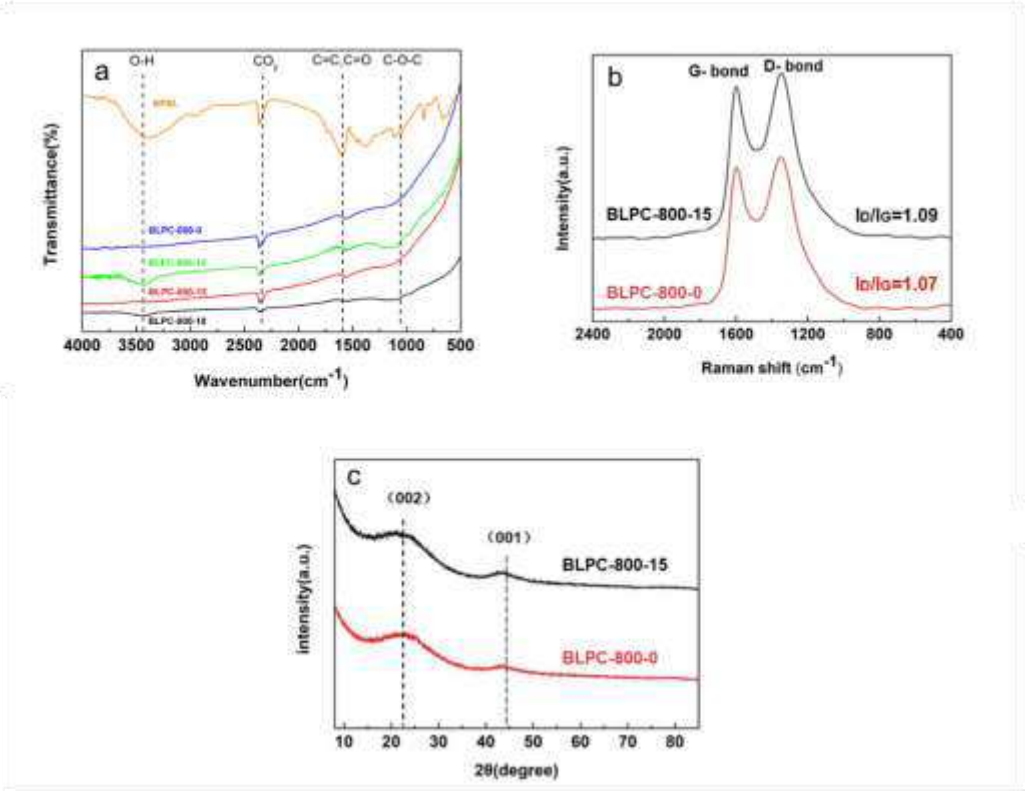

Fig. 4. FTIR spectra of BPBL and BLPC (a); Raman spectra of BLPC (b); XRD patterns of BLPC-800-0 and BLPC-800-15 (c).

3.3 Adsorptive property

Fig.5 shows adsorption capacities of TCH and MG onto the BLPC-T-x at 298 K. The effect of activation temperature and BPBL/KOH ratio on adsorption performance were investigated. Obviously, the improvement of adsorption performance of BLPC is related to the ratio of KOH, the adsorption capacities of the prepared BLPC for TCH are 487, 733, 884 and 738 mg/g, and the adsorption capacities for MG are 678, 933, 1084 and 942 mg/g when the addition ratio of KOH is 0, 12, 15 and 18 % at 750 °C, respectively.

The adsorption capacity of BLPC increases at higher activation temperature, but decreases when the activation temperature exceeds 762°C (the boiling point of K), because KOH is reduced to free metallic K. Free metal K can be embedded in the carbon and widen the space between the carbon layers, increasing specific surface area of BLPC. Therefore, the adsorption performance of BLPC for TCH and MG is improved when the activation temperature rises from 750°C to 800°C, the adsorption performance decreases when the activation temperature rises to 850 °C. It can be seen from Fig. 5 that the adsorption capacity of BLPC-800-15 for TCH and MG is 1047 mg/g 1277 mg/g, respectively, implying that the BLPC-800-15 exhibits excellent adsorption performance. Fig. 5c.d lists the comparison of the adsorption performance of BLPC-800-15 on TCH and MG with other porous carbon adsorbents. It can be observed that the adsorption capacities of BLPC-800-15 for both two pollutants are significantly higher than that of adsorbents recently reported[29-42], illustrating that the prepared BLPC-800-15 is a promising adsorbent for the removal of antibiotics and dyes.

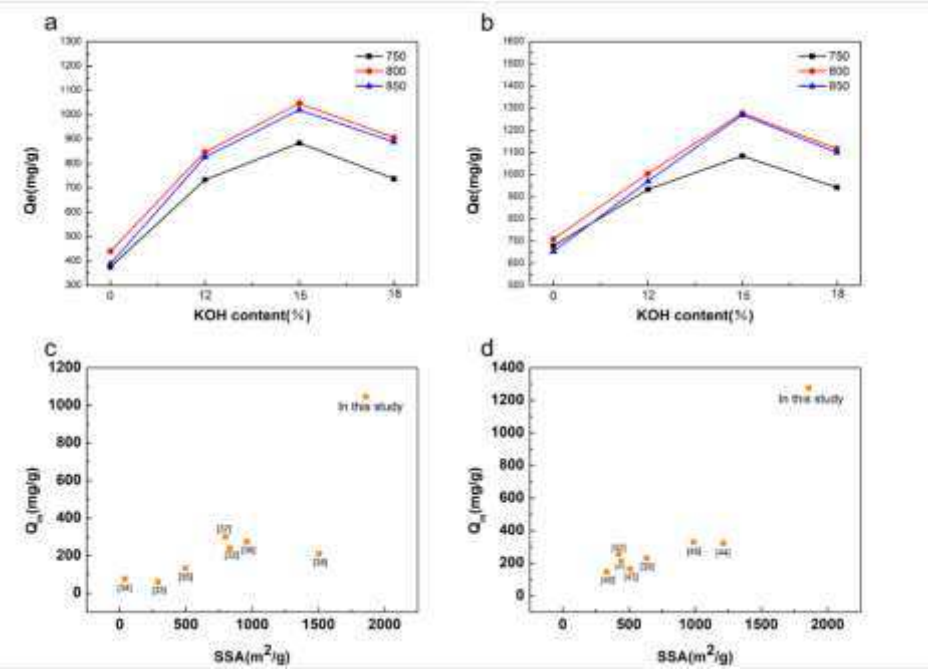

Fig. 5. The comparisons of TCH (a) and MG (b) adsorption by BLPC-T-x adsorbents, the comparison of specific surface area and adsorption capacity of TCH (c) and MG (d) with different adsorbents.

3.4 Desorption experiments

The recycling performance of adsorbents is a critical parameter in practical and commercial applications. The adsorbed BLPC was desorbed by ethanol ultrasonic desorption for four consecutive adsorption-desorption experiments, and the results are shown in Fig.6a. The adsorption efficiency of TCH and MG on porous carbon still possesses 81.1 % and 85.2 % after four cycles, respectively, indicating the satisfactory cycle performance of BLPC-800-15. Removal efficiency of BLPC-800-15 in actual waterbodies are required to be studied. Fig. 6b shows the adsorption efficiency of BLPC for TCH and MG in tap water, river water and seawater. The results show that the adsorption capacity of the two pollutants in tap water is close to deionized water, and the adsorption capacity of BLPC to TCH and MG is 1043 and

1277 mg/g, respectively. Additionally, removal efficiencies of TCH and MG slightly decrease using river and sea as water resources, and the adsorption capacities of BLPC to TCH and MG in sea water are 936 and 1186 mg/g, respectively, and that in river water are 879 and 1103 mg/g, respectively. The main reason may be the existence of natural organic matter in rivers and seawater[43], which competes with the adsorption of BLPC for TCH and MG.

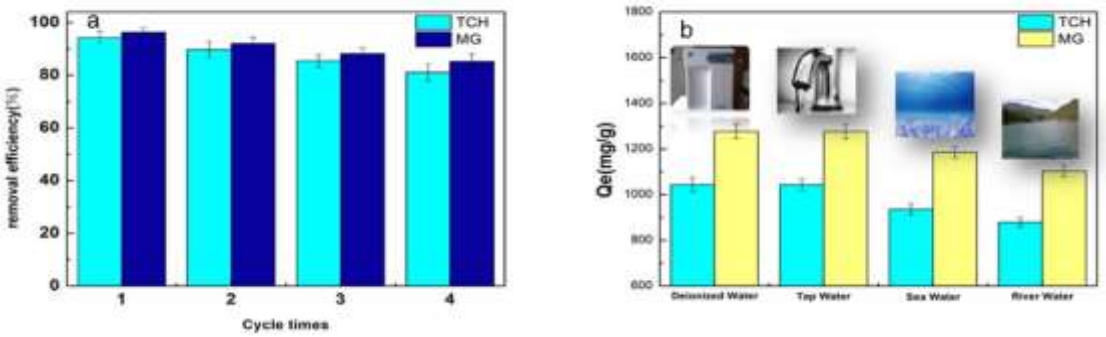

Fig. 6. Regeneration performance of BLPC-800-15 for TCH and MG removal (a), the adsorption of TCH and MG by BLPC-800-15 in different water-body (b).

3.5 Adsorption kinetics of TCH and MG onto BLPC

Kinetic studies of adsorption play an important role in understanding adsorption dynamics and mechanism through order of rate constant. Two different concentrations (1000 and 1500 mg/L) and three different temperature (288, 298 and 308 K) were used to study the adsorption kinetics with data fitted using pseudo-first-order and pseudo-second-order for both TCH and MG (Fig. 7). It can be observed that the adsorption capacity of BLPC increases sharply within 100 min due to pore filling, and then increases slightly until equilibrium reaches. Almost all the adsorption processes can reach equilibrium within 200 min, indicating the efficient adsorption capacity of as-prepared adsorbent. As the temperature rises from 288 K to 308 K, the adsorption capacity of BLPC for TCH and MG increases continuously because the adsorption of TCH and MG is an endothermic process[44, 45]. The results indicates that the rise of temperature helps for adsorption of pollutants. The models of pseudo-first-order and pseudo-second-order were used to analyze the adsorption kinetics of BLPC for TCH and MG according to Equations (8) and (9), respectively.

$$Q_t = q_e \times (1 - e^{-K_1 t}) \quad (8)$$

$$Q_t = \frac{q_e^2 K_2 t}{1 + q_e K_2 t} \quad (9)$$

q_t (mg/g) is the amount of TCH and MG adsorbed at t (min), and q_e (mg/g) represents the amount of TCH and MG adsorption at equilibrium. K_1 (min^{-1}) is the pseudo-first-order adsorption rate constant. K_2 (min^{-1}) is the pseudo-second-order adsorption rate constant. $Q_{e,cal}$ and $Q_{e,exp}$ represent theoretical adsorption capacity and actual adsorption capacity, respectively. Fitting results of adsorption kinetics are shown in Fig. 7 and the detailed kinetics parameters are presented in Table 2 and Table 3. It can be seen from Table 2 and Table 3 that R^2 value of the pseudo-second-order rate model is higher (>0.95). In addition, the value of $Q_{e,cal}$ obtained by the pseudo-second-order rate model is close to $Q_{e,exp}$

value. Therefore, the pseudo-second order model is suitable for describing the adsorption kinetics of TCH and MG on BLPC-800-15.

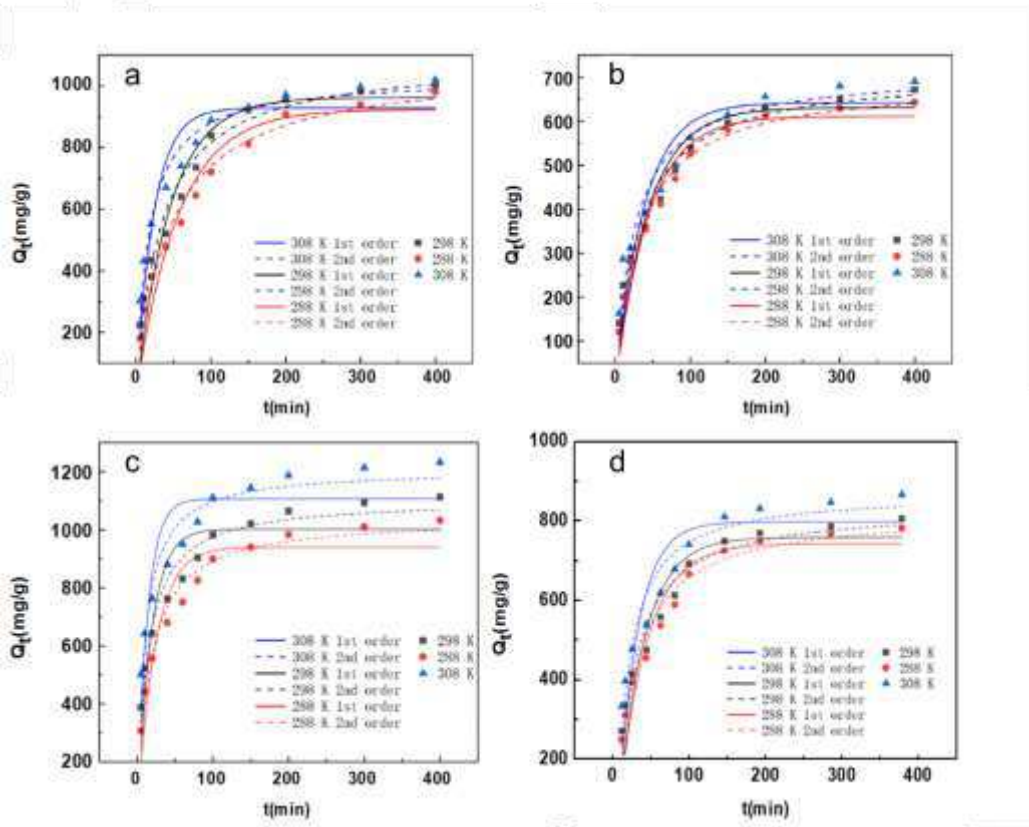

Fig. 7. Time profiles of adsorption of TCH (a，b) and MG (c，d) onto BLPC-800-15 at the different initial solution concentration and temperature and the corresponding fitting curves of the pseudo-first-order rate model and the pseudo-second-order rate model.

Table 2 Kinetics parameters for the adsorption of TCH onto porous carbon at the different conditions

			Pseudo-first-order model			Pseudo-second-order model		
C_o(mg/L)	T (K)	$Q_{e,exp}$ (mg/g)	$k_1(10^{-2}$ $min^{-1})$	$Q_{e,cal}$ (mg/g)	R^2	$k_2(10^{-3}$ $min^{-1})$	$Q_{e,cal}$ (mg/g)	R^2
1000	288	634	2.26	611.41	0.94	0.044	692.90	0.98
	298	660	2.28	631.05	0.92	0.044	711.38	0.97
	308	682	2.60	642.44	0.86	0.054	713.88	0.95
1500	288	980	2.20	929.0	0.93	0.018	1029.15	0.97
	298	1002	1.76	924.4	0.93	0.021	1063.21	0.97
	308	1020	4.21	963.0	0.87	0.027	1088.88	0.97

Table 3 Kinetics parameters for the adsorption of MG onto porous carbon at the different conditions

C_o(mg/L)	T (K)	$Q_{e,exp}$ (mg/g)	Pseudo-first-order model			Pseudo-second-order model		
			$k_1(10^{-2}$ $min^{-1})$	$Q_{e,cal}$ (mg/g)	R_2	$k_2(10^{-3}$ $min^{-1})$	$Q_{e,cal}$ (mg/g)	R^2
1000	288	820	2.60	775.42	0.86	0.033	841.33	0.96
	298	863	2.73	903.21	0.88	0.036	890.12	0.96
	308	942	3.57	854.32	0.90	0.046	957.11	0.95
1500	288	1032	4.11	939.5	0.89	0.057	1039.98	0.97
	298	1113	3.52	1001.8	0.86	0.069	1102.90	0.97
	308	1232	7.40	1105.9	0.87	0.083	1206.32	0.98

3.6 Adsorption isotherm

Two adsorption isotherms namely the Langmuir and Freundlich isotherms were used to analyze mechanism for the adsorption of TCH and MG onto BLPC-800-15. The Langmuir isotherm assumes monolayer coverage of adsorbate over a homogenous adsorbent surface. The Langmuir equation represents the reference (10).

$$Q_e = \frac{Q_o K_t C_e}{1+K_t C_e} \quad (10)$$

Q_e (mg/g) is adsorption capacity of adsorbent per unit mass under equilibrium state. Q_o (mg/g) is the maximum adsorption capacity. K_t (L/mg) represents Langmuir adsorption constant and C_e (mg/L) stands for equilibrium concentration of TCH and MG. The Freundlich isotherm assumes multilayer coverage of adsorbate over adsorbent surface. The Freundlich equation represents the reference (11).

$$Q_e = K_F C_e^{\frac{1}{n}} \quad (11)$$

Q_e (mg/g) is the adsorption amount of adsorbent per unit mass under the equilibrium state. C_e (mg/L) is the equilibrium concentration. K_F and n are Freundlich constants, which represent adsorption capacity and adsorption intensity of the adsorbent, respectively. The adsorption isotherm fitted with Langmuir and Freundlich models are illustrated in Fig. 8 and the calculated parameters are listed in Table 4 and Table 5. The adsorption capacity of porous carbon increases with the rise of TCH and MG initial concentration and temperature. It can be seen from Table 4 and Table 5 that R^2 values calculated from Langmuir model is higher than that from Freundlich model for both TCH and MG at 288 K, 398 K and 308 K, indicating that monomolecular layer adsorption plays a major role in adsorption of TCH and MG on BLPC. Q_m values of Langmuir isotherm for TCH are 1050, 1171 and 1215 mg/g at 288, 298 and 308 K, respectively. Additionally, Q_m values of Langmuir isotherm for MG are 1218, 1284 and 1435 mg/g, respectively. An increase of Q_m values at higher temperature indicates that higher temperature is beneficial for adsorption. Generally, K_F parameter is used to evaluate

the adsorption capacity and large K_F value suggests high adsorption capacity of the adsorbent. K_F value is directly proportional to temperature, indicating that high temperature is favorable for adsorption.

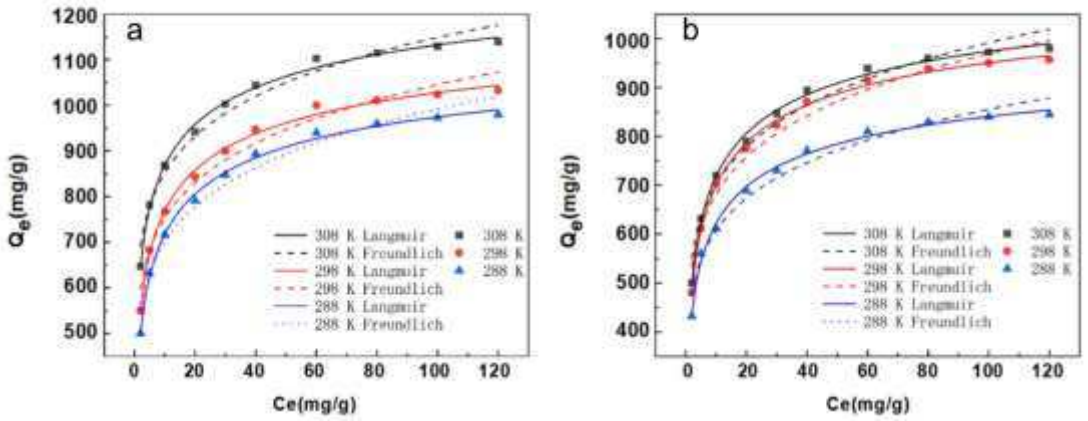

Fig. 8. Adsorption isotherms of TCH(a)and MG(b) onto BLPC-800-15 at 288 K, 298 K and 308 K and their corresponding curves fitted by Langmuir and Freundlich models

Table 4 Isotherm parameters for the adsorption of TCH onto BLPC-800-15

Model		Langmuir		Freundlich	
T (K)	Q_m (mg/g)	K_L (L/mg)	R^2	K_F (L/g)	R^2
288	1050.15	0.53	0.99	431.27	0.97
298	1171.10	0.51	0.99	479.06	0.97
308	1215.15	0.517	0.99	495.64	0.97

Table 5 Isotherm parameters for the adsorption of TCH onto BLPC-800-15

		Langmuir		Freundlich	
T (K)	Q_m (mg/g)	K_L (L/mg)	R^2	K_F (L/g)	R^2
288	1218.81	0.51	0.99	495.04	0.97
298	1284.20	0.56	0.99	541.72	0.97
308	1435.78	0.63	0.99	632.32	0.97

3.7 Effect of pH value on adsorption of the porous carbon

In order to further investigate effect of pH values on adsorption of TCH and MG, the adsorption capacity of BLPC to TCH and MG at different pH values was determined. The adsorption capacity of BLPC to TCH reaches the maximum at pH = 7 (Fig. 9b). TCH mainly exists in the form of TCH_3^+ when pH is less than 7. However, TCH is mainly converted

into the state of TCH_2, TCH^- and TC^{2-} under neutral and alkaline conditions. Therefore, electrostatic repulsion inhibits the TCH adsorption on the BLPC because porous carbon has a positive charge when pH is less than 4.1 as shown in Fig. 9a.b. On the contrary, the electrostatic interaction between TCH and BLPC increase at high pH value, leading to an increase in TCH adsorption capacity. Surfaces of BLPC are negatively charged at pH above 4.1. The electrostatic repulsion between TCH and negatively charged BLPC results in reduction of the adsorption capacity of BLPC to TCH. It can be seen from Fig. 9c that removal capacity for MG increases when pH rises from 3 to 9. The adsorption rate remains stable when the pH value ranges from 9 to11, As MG is a cationic dye, the adsorption capacity decreases with the rise of the positive charge on the surface of BLPC., both the surface of BLPC and MG are positively charged and the adsorption performance is relatively low when the pH is less than 4.1.The negative charge on the surface of BLPC increases at higher pH, and the electrostatic adsorption is improved, leading to the enhancement of the adsorption performance, and the adsorption effect of BLPC for dyes is mainly affected by the electrostatic interaction between pollutants and the surface of BLPC. The increase in the number of H^+ ions in aqueous solution further weakens the adsorption capacity, and H^+ ions occupy the active site on the surface of BLPC, limiting its interaction with cationic dye molecules.

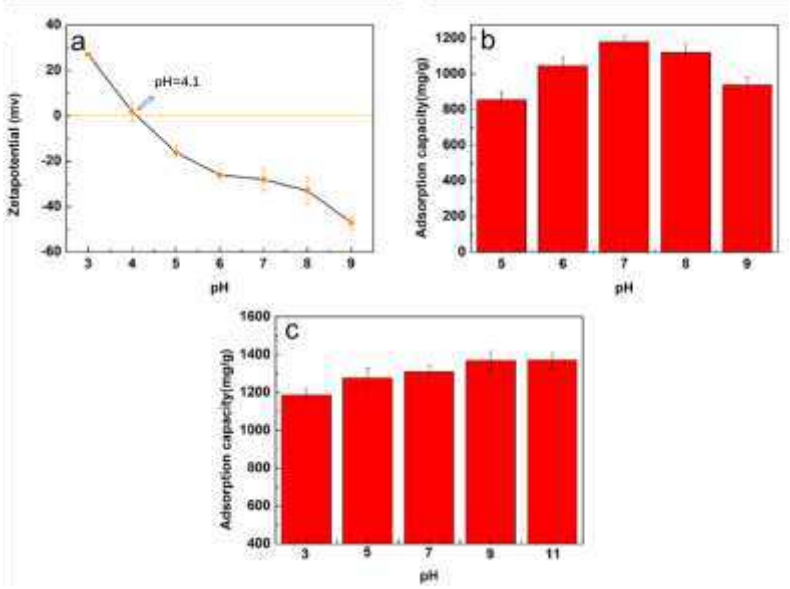

Fig. 9. Zeta potential of BLPC-800-15 at different pH value conditions(a), adsorption performance of TCH at different pH value conditions(b), adsorption performance of MG at different pH value conditions(c)

3.8 Adsorption mechanism

The adsorption mechanism of BLPC for TCH and Mg is not only the pore filling caused by high specific surface area, but also other adsorption mechanisms. In addition, BLPC surface is negatively charged when pH is higher than pH_{pzc} as shown in Fig. 10. TCH and MG with positive charge are easily attracted by static electricity and adsorbed on the surface of BLPC. The carboxyl group and hydroxyl group in BLPC act as hydrogen donors and is bonded with the H-bond receptor between TCH and MG to produce hydrogen bond interaction. In addition, π-π interaction between the benzene

ring on BLPC and TCH and MG contributes to adsorption of TCH and MG on BLPC[46]. TCH and MG molecule has a large flat ring structure and may form van der Waals force on the surface of BLPC, leading to further adsorption.

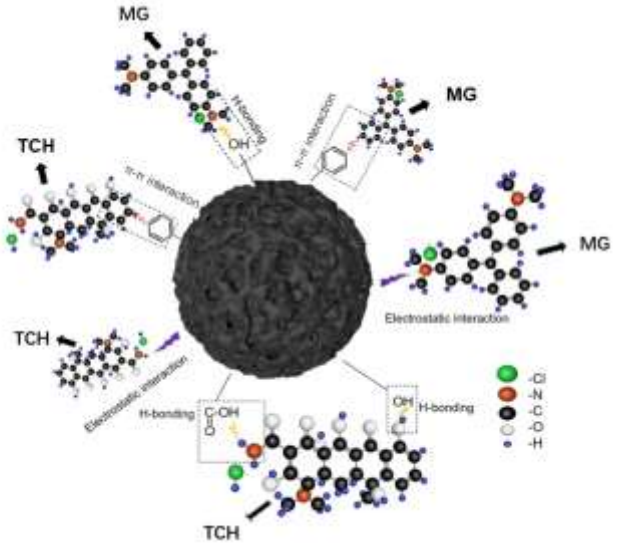

Fig. 10. TCH and MG adsorption mechanism

3.9 Photo-thermal adsorption property

For highly efficient solar energy promoted adsorption, it is very important to develop photothermal materials that efficiently absorb solar light and convert to thermal energy. Higher content of graphite in BLPC, thus it has a higher light absorption rate in the infrared region, and can be heated up rapidly in a short time under the irradiation of near infrared lamp. As shown in Fig.11a, BLPC has fast heating response and good photothermal performance. Fig. 11(c-e) shows infrared images of saturation temperature on the BLPC surface at distances of 60 cm, 50 cm, and 40 cm, the surface temperature of BLPC is significantly higher than the ambient temperature. Fig.11b shows the comparison of the adsorption performance of BLPC on TCH and MG without or with light. It can be seen that the adsorption capacity of BLPC on TCHE and MG at 50min is 552 and 790 mg/g, respectively, and the adsorption capacity of BLPC on TCH and MG at near infrared light is 584 and 847mg/g, respectively. The excellent photothermal effect of BLPC surface can be applied to promote the adsorption efficiency of outdoor solar energy.

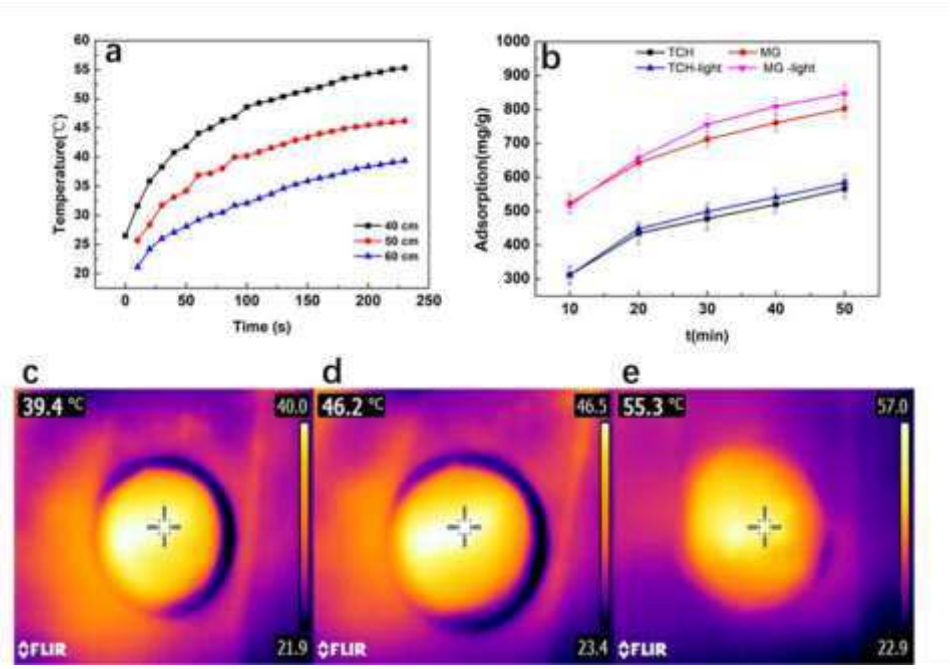

Fig. 11. (a) The temperature of BLPC under different illumination time and illumination distance, (b) adsorption rate of porous carbon with or without light contrast, (c-e) infrared images of porous carbon saturation temperature were obtained at 40 cm, 50 cm and 60 cm, respectively.

4. Conclusion

The BPBL waste residue was fully utilized to convert BPBL into porous carbon by one step activation at high temperature by KOH. The specific surface area of the prepared BLPC is 1859.08 m^2/g, and the adsorption capacity of THE BLPC to TCH and MG is 1047 and 1277 mg /g, respectively. In addition, BLPC can improve the adsorption properties of TCH and MG under near-infrared light due to the photothermal effect of BLPC and can be applied to promote the adsorption effect under outdoor solar light. BLPC could be regarded as a promising adsorbent for adsorptive purification of TCH and MG wastewater.

Acknowledgement

This work was financially supported by the Science and Technology Planning Project of Sichuan Province (No. 2020YFN0150).

Conflict of interest

The authors declare that no conflict of interest exits in the submission of this manuscript, and manuscript has approved by all authors for publication. We would like to declare that the work was original research that has not been published

previously, and not under consideration for publication elsewhere in whole or in part. All the authors listed have approved the manuscript that is enclosed.

References

[1] A.M. Voigt, N. Zacharias, C. Timm, F. Wasser, E. Sib, D. Skutlarek, M. Parcina, R.M. Schmithausen, T. Schwartz, N. Hembach, A. Tiehm, C. Stange, S. Engelhart, G. Bierbaum, T. Kistemann, M. Exner, H.A. Faerber, C. Schreiber, Association between antibiotic residues, antibiotic resistant bacteria and antibiotic resistance genes in anthropogenic wastewater – An evaluation of clinical influences, Chemosphere, 241 (2020) 125032.

[2] X. Zheng, Y. Li, H. Peng, Z. Huang, H. Wang, J. Wen, Efficient solar-light photodegradation of tetracycline hydrochloride using BiVO4/MoO3 composites, Colloids and Surfaces A: Physicochemical and Engineering Aspects, 621 (2021) 126599.

[3] S. Mohapatra, S.S. Mishra, P. Bhalla, H. Thatoi, Engineering grass biomass for sustainable and enhanced bioethanol production, Planta, 250 (2019) 395-412.

[4] L. Zhao, Y.H. Dong, H. Wang, Residues of veterinary antibiotics in manures from feedlot livestock in eight provinces of China, Science of The Total Environment, 408 (2010) 1069-1075.

[5] J. Wang, L. Jiang, F. Liu, M. Jia, M. Liu, J. Li, Y. Lai, Enhanced photoelectrochemical degradation of tetracycline hydrochloride with FeOOH and Au nanoparticles decorated WO3, Chemical Engineering Journal, 407 (2021) 127195.

[6] X. Zhao, X. Li, Y. Li, X. Zhang, F. Zhai, T. Ren, Y. Li, Metagenomic analysis reveals functional genes in soil microbial electrochemical removal of tetracycline, Journal of Hazardous Materials, 408 (2021) 124880.

[7] C. Pizan-Aquino, A. Wong, L. Avilés-Félix, S. Khan, G. Picasso, M.D.P.T. Sotomayor, Evaluation of the performance of selective M-MIP to tetracycline using electrochemical and HPLC-UV method, Materials Chemistry and Physics, 245 (2020) 122777.

[8] Y. Wang, H. Fan, P. Keung Wong, Y. Wu, B. Rittmann, Biodegradation of tetracycline using hybrid material (UCPs-TiO2) coupled with biofilms under visible light, Bioresource Technology, 323 (2021) 124638.

[9] X. Gao, Y. Chen, Z. Kang, B. Wang, L. Sun, D.-P. Yang, W. Du, Enhanced degradation of aqueous tetracycline hydrochloride by integrating eggshell-derived CaCO3/CuS nanocomposite with advanced oxidation process, Molecular Catalysis, 501 (2021) 111380.

[10] Z. Yang, Z. Zhao, X. Yang, Z. Ren, Xanthate modified magnetic activated carbon for efficient removal of cationic dyes and tetracycline hydrochloride from aqueous solutions, Colloids and Surfaces A: Physicochemical and Engineering Aspects, 615 (2021) 126273.

[11] H. Yang, H. Yu, J. Wang, T. Ning, P. Chen, J. Yu, S. Di, S. Zhu, Magnetic porous biochar as a renewable and highly effective adsorbent for the removal of tetracycline hydrochloride in water, Environmental Science and Pollution Research, (2021).

[12] A.M. Pandele, H. Iovu, C. Orbeci, C. Tuncel, F. Miculescu, A. Nicolescu, C. Deleanu, S.I. Voicu, Surface modified cellulose acetate membranes for the reactive retention of tetracycline, Separation and Purification Technology, 249 (2020) 117145.

[13] H. Zhang, T. Lu, M. Wang, R. Jin, Y. Song, Y. Zhou, Z. Qi, W. Chen, Inhibitory role of citric acid in the adsorption of tetracycline onto biochars: Effects of solution pH and Cu2+, Colloids and Surfaces A: Physicochemical and Engineering Aspects, 595 (2020) 124731.

[14] J. Miao, F. Wang, Y. Chen, Y. Zhu, Y. Zhou, S. Zhang, The adsorption performance of tetracyclines on magnetic graphene oxide: A novel antibiotics absorbent, Applied Surface Science, 475 (2019) 549-558.
[15] J. Dai, X. Meng, Y. Zhang, Y. Huang, Effects of modification and magnetization of rice straw derived biochar on adsorption of tetracycline from water, Bioresource Technology, 311 (2020) 123455.
[16] C. Chen, D. Chen, S. Xie, H. Quan, X. Luo, L. Guo, Adsorption Behaviors of Organic Micropollutants on Zirconium Metal–Organic Framework UiO-66: Analysis of Surface Interactions, ACS Applied Materials & Interfaces, 9 (2017) 41043-41054.
[17] J. Rivera-Utrilla, G. Prados-Joya, M. Sánchez-Polo, M.A. Ferro-García, I. Bautista-Toledo, Removal of nitroimidazole antibiotics from aqueous solution by adsorption/bioadsorption on activated carbon, Journal of Hazardous Materials, 170 (2009) 298-305.
[18] Y. Ren, H. Cao, H. Xu, X. Xiong, R. Krastev, L. Liu, Improved aging properties of bio-bitumen coating sheets by using modified lignin, Journal of Environmental Management, 274 (2020) 111178.
[19] F. Liu, Z. Wang, H. Zhang, L. Jin, X. Chu, B. Gu, H. Huang, W. Yang, Nitrogen, oxygen and sulfur co-doped hierarchical porous carbons toward high-performance supercapacitors by direct pyrolysis of kraft lignin, Carbon, 149 (2019) 105-116.
[20] J. He, P. Ma, A. Xie, L. Gao, Z. Zhou, Y. Yan, J. Dai, C. Li, From black liquor to highly porous carbon adsorbents with tunable microstructure and excellent adsorption of tetracycline from water: Performance and mechanism study, Journal of the Taiwan Institute of Chemical Engineers, 63 (2016) 295-302.
[21] Y. Gao, Q. Yue, B. Gao, A. Li, Insight into activated carbon from different kinds of chemical activating agents: A review, Science of The Total Environment, 746 (2020) 141094.
[22] M.A. Al-Ghouti, D.A. Da'ana, Guidelines for the use and interpretation of adsorption isotherm models: A review, Journal of Hazardous Materials, 393 (2020) 122383.
[23] M. Gil, S. Pasieczna-Patkowska, P. Nowicki, Application of microwave heating in the preparation of functionalized activated carbons, Adsorption, 25 (2019) 327-336.
[24] A.H. Jawad, K. Ismail, M.A.M. Ishak, L.D. Wilson, Conversion of Malaysian low-rank coal to mesoporous activated carbon: Structure characterization and adsorption properties, Chinese Journal of Chemical Engineering, 27 (2019) 1716-1727.
[25] S. Wu, H. He, X. Li, C. Yang, G. Zeng, B. Wu, S. He, L. Lu, Insights into atrazine degradation by persulfate activation using composite of nanoscale zero-valent iron and graphene: Performances and mechanisms, Chemical Engineering Journal, 341 (2018) 126-136.
[26] X. Wei, S. Wan, S. Gao, Self-assembly-template engineering nitrogen-doped carbon aerogels for high-rate supercapacitors, Nano Energy, 28 (2016) 206-215.
[27] X. Jiao, L. Zhang, Y. Qiu, J. Guan, Comparison of the adsorption of cationic blue onto graphene oxides prepared from natural graphites with different graphitization degrees, Colloids and Surfaces A: Physicochemical and Engineering Aspects, 529 (2017) 292-301.
[28] J. Hou, K. Jiang, M. Tahir, X. Wu, F. Idrees, M. Shen, C. Cao, Tunable porous structure of carbon nanosheets derived from puffed rice for high energy density supercapacitors, Journal of Power Sources, 371 (2017) 148-155.
[29] Y. Cai, L. Liu, H. Tian, Z. Yang, X. Luo, Adsorption and Desorption Performance and Mechanism of Tetracycline Hydrochloride by Activated Carbon-Based Adsorbents Derived from Sugar Cane Bagasse Activated with ZnCl2, Molecules, 24 (2019) 4534.

[30] D. Zhang, Q. He, X. Hu, K. Zhang, C. Chen, Y. Xue, Enhanced adsorption for the removal of tetracycline hydrochloride (TC) using ball-milled biochar derived from crayfish shell, Colloids and Surfaces A: Physicochemical and Engineering Aspects, 615 (2021) 126254.
[31] G.A. Haghighat, M.H. Saghi, I. Anastopoulos, A. Javid, A. Roudbari, S.S. Talebi, S.K. Ghadiri, D.A. Giannakoudakis, M. Shams, Aminated graphitic carbon derived from corn stover biomass as adsorbent against antibiotic tetracycline: Optimizing the physicochemical parameters, Journal of Molecular Liquids, 313 (2020) 113523.
[32] H.M. Jang, S. Yoo, Y.-K. Choi, S. Park, E. Kan, Adsorption isotherm, kinetic modeling and mechanism of tetracycline on Pinus taeda-derived activated biochar, Bioresource Technology, 259 (2018) 24-31.
[33] H.M. Jang, E. Kan, Engineered biochar from agricultural waste for removal of tetracycline in water, Bioresource Technology, 284 (2019) 437-447.
[34] M.J. Ahmed, M.A. Islam, M. Asif, B.H. Hameed, Human hair-derived high surface area porous carbon material for the adsorption isotherm and kinetics of tetracycline antibiotics, Bioresource Technology, 243 (2017) 778-784.
[35] A.A. Ahmad, A.T.M. Din, N.K.E.M. Yahaya, A. Khasri, M.A. Ahmad, Adsorption of basic green 4 onto gasified Glyricidia sepium woodchip based activated carbon: Optimization, characterization, batch and column study, Arabian Journal of Chemistry, 13 (2020) 6887-6903.
[36] H.N. Bhatti, A. Jabeen, M. Iqbal, S. Noreen, Z. Naseem, Adsorptive behavior of rice bran-based composites for malachite green dye: Isotherm, kinetic and thermodynamic studies, Journal of Molecular Liquids, 237 (2017) 322-333.
[37] M. Yu, Y. Han, J. Li, L. Wang, CO2-activated porous carbon derived from cattail biomass for removal of malachite green dye and application as supercapacitors, Chemical Engineering Journal, 317 (2017) 493-502.
[38] E. Akar, A. Altinişik, Y. Seki, Using of activated carbon produced from spent tea leaves for the removal of malachite green from aqueous solution, Ecological Engineering, 52 (2013) 19-27.
[39] V.K. Singh, A.B. Soni, R.K. Singh, Process Optimization Studies of Malachite Green dye Adsorption onto Eucalyptus (Eucalyptus globulus) Wood Biochar using Response Surface Methodology, Oriental Journal of Chemistry, 32 (2016) 2621-2631.
[40] H. Zhang, F. Zhang, Q. Huang, Highly effective removal of malachite green from aqueous solution by hydrochar derived from phycocyanin-extracted algal bloom residues through hydrothermal carbonization, RSC Advances, 7 (2017) 5790-5799.
[41] A.P. Rawat, D.P. Singh, Decolourization of malachite green dye by mentha plant biochar (MPB): A combined action of adsorption and electrochemical reduction processes, Water Science and Technology, 77 (2018) 1734-1743.
[42] M.A. Ahmad, R. Alrozi, Removal of malachite green dye from aqueous solution using rambutan peel-based activated carbon: Equilibrium, kinetic and thermodynamic studies, Chemical Engineering Journal, 171 (2011) 510-516.
[43] Z. Zhao, X. Cheng, X. Hua, B. Jiang, C. Tian, J. Tang, Q. Li, H. Sun, T. Lin, Y. Liao, G. Zhang, Emerging and legacy per- and polyfluoroalkyl substances in water, sediment, and air of the Bohai Sea and its surrounding rivers, Environmental Pollution, 263 (2020) 114391.
[44] H. Yang, H. Yu, J. Wang, T. Ning, P. Chen, J. Yu, S. Di, S. Zhu, Magnetic porous biochar as a renewable and highly effective adsorbent for the removal of tetracycline hydrochloride in water, Environmental Science and Pollution Research, 28 (2021) 61513-61525.
[45] W. Qu, T. Yuan, G. Yin, S. Xu, Q. Zhang, H. Su, Effect of properties of activated carbon on malachite green adsorption, Fuel, 249 (2019) 45-53.
[46] G. Sharma, S. Sharma, A. Kumar, M. Naushad, B. Du, T. Ahamad, A.A. Ghfar, A.A. Alqadami, F. J.Stadler, Honeycomb structured activated carbon synthesized from Pinus roxburghii cone as effective bioadsorbent for toxic malachite green dye, Journal of Water Process Engineering, 32 (2019) 100931.